A COLLISIONAL TREATMENT OF THE TRAPPED PARTICLE MODE IN MULTI-REGION MIRROR SYSTEMS

by

H. Ramachandran, A. J. Lichtenberg,
M. A. Lieberman, and A. K. Sen

Memorandum No. UCB/ERL M87/16

18 March 1987

A COLLISIONAL TREATMENT OF THE TRAPPED PARTICLE MODE IN MULTI-REGION MIRROR SYSTEMS

by

H. Ramachandran, A. J. Lichtenberg,
M. A. Lieberman, and A. K. Sen

Memorandum No. UCB/ERL M87/16

18 March 1987

ELECTRONICS RESEARCH LABORATORY

College of Engineering
University of California, Berkeley
94720

A COLLISIONAL TREATMENT OF THE TRAPPED PARTICLE MODE IN MULTI-REGION MIRROR SYSTEMS

by

H. Ramachandran, A. J. Lichtenberg,
M. A. Lieberman, and A. K. Sen

Memorandum No. UCB/ERL M87/16

18 March 1987

ELECTRONICS RESEARCH LABORATORY

College of Engineering
University of California, Berkeley
94720

A Collisional Treatment of the Trapped Particle Mode in Multi-Region Mirror Systems

H.Ramachandran , A.J.Lichtenberg , M.A.Lieberman
Department of Electrical Engineering and Computer Sciences
University of California,Berkeley,CA 94720

A.K.Sen
Department of Electrical Engineering
Columbia University,New York,NY 10027

Abstract

A method of analysis has been developed for treating the trapped particle mode in magnetic mirror systems in which three or more spatially distinct regions are present. The method applies for plasmas in which the electrons are sufficiently collisional that a Krook collision operator can be used. The ions have been treated as trapped within individual regions. The approximations allow the problem to be reduced to coupled algebraic equations, that are solved numerically. The numerical solutions are compared with asymptotic analytic solutions including known results. The results are applied to the multiple mirror experiment at Berkeley, which has three mirror cells of equal length but variable density, in which the central cell contains a potential barrier produced by a hot electron distribution.

I Introduction

Mirror machines that are MHD stable (having net good curvature) can become unstable due to the presence of velocity space barriers such as local potentials or magnetic mirrors. The net good curvalure criterion assumes that communication between regions of local good and bad curvature is strong enough so that only an integrated criterion is needed. However in systems with barriers to the particle flow, this communication is via passing (or transiting) particles. The number density of passing particles can become much smaller than the overall density. This gives rise to the trapped particle instability in which the unstable part of the machine goes unstable via a localized mode.

The curvature driven trapped particle instability is important in mirror machines and has been well studied in recent years . The early work[1] dealt with collisionless systems. Here, it is possible to find a threshold passing fraction above which the system is stable with respect to this mode. More recent studies[2345] have dealt with collisional systems. Here, the mode is always unstable. The question is only whether the growth rate is small enough that non-linear processes or neglected aspects in the modelling of the system saturate or stabilize the mode. These studies were done using a pitch-angle scattering operator as the collision operator, or else worked in an asymptotic regime where one process dominated the behaviour. In this paper we examine a new collisional regime, such that pitch angle scattering competes with drag and energy scattering effects. The collision frequency is assumed large enough to allow the use of a Krook-type operator. The motivation for this work comes from the curvature driven trapped particle

mode measurements performed on the multiple mirror experiment (MMX).[6]

The model and the underlying assumptions are discussed in section II, and the dispersion equation derived in section III. Analytical limits and approximations are obtained in section IV, using perturbation theory. We discuss the numerical results in section V and conclude with remarks on generalizations and limitations of the theory.

II Theoretical Model

The analysis is motivated by the multiple mirror experiment (MMX) [6], shown schematically in fig. 1. It consists of a linear set of connected mirror cells. A variety of mirror and quadrature coils allow the magnetic field curvature within any cell to be varied from unstable (axisymmetric mirrors) to stable (quadrupoles or cusps). In the experiments, three cells are used as shown in the figure. Cell 1 by itself is unstable and cell 3 is stable. Cell 2 is mildly stable. The entire three cell system is stable to flute modes. The mirror ratio is three. The plasma density is about 10^{12} cm^{-3}, and the electron and ion temperatures are about 5 eV. The experiment involves suddenly creating a magnetically confined hot electron species in the middle cell, using short pulse ($\sim$ 3 μsec) electron cyclotron resonance heating (ECRH). Nearly all the electrons in the ECRH cell are heated. The electrons in the other cells are also affected to a smaller extent - their temperature jumps to about 15 eV after the pulse. As a result, an electrostatic (thermal) barrier appears and impedes the cold electron flow between cell 1 and cell 3. It is observed that this barrier drives the system unstable. The plasma in cell 1 (unstable by itself) experiences a curvature driven trapped particle instability (localized and flute-like), while the plasma in the other cells remains stable.

The analysis of this phenomenon is complicated by the fact that several relevant frequencies of the system are of the same order. For example the ion bounce frequency ($\sim l/v_i$, where l is the machine length, and v_i is the ion thermal velocity) is close to but somewhat smaller than the mode frequency

ω. The diamagnetic drift frequency ($\omega_* \sim T_e/r_p^2 B \sim 3 \times 10^5$ sec^{-1}) is comparable to electron collision frequency ($\nu_e \sim 2.9 \times 10^{-6} n \lambda T_e^{-1.5}$ sec^{-1} $\sim 6.6 \times 10^5$ sec^{-1}). . The hot-electron drift frequency ($\omega_{dh} \sim \langle v_\parallel^2 + v_\perp^2/2 \rangle_h / \Omega_{ce} R_B \sim 2 \times 10^5$ sec^{-1}) is of the same order. The pitch angle scattering time for electrons to scatter into and out of the loss-cone is about equal to the drag time for the same process. Some of the other parameters of the system are as follows: the MHD growth rate in the unstable cell is

$$\gamma \sim \left[\omega_*(|\omega_{di}| + |\omega_{de}|)/b_i(\frac{T_e}{T_i})\right]^{\frac{1}{2}} \sim 10^5 \text{ sec}^{-1}$$

The cold electron drift frequency is $\omega_{de} \sim \langle v_\parallel^2 + v_\perp^2/2 \rangle_e / \Omega_{ce} R_B \sim 2 \times 10^3$ sec^{-1}. The ion drift frequency is $\omega_{di} \sim \langle v_\parallel^2 + v_\perp^2/2 \rangle_i / \Omega_{ci} R_B \sim 2 \times 10^3$ sec^{-1}. Here T_e, T_i are the cold electron and ion temperatures in eV (~ 5 eV), r_p the nominal plasma radius, B the background magnetic field, n_0 the plasma density, λ the coulomb logarithm, p the fluid pressure, n the fluid density, R_b the radius of curvature of the magnetic lines, $\Omega_{ce,i}$ the cyclotron frequency, and $b_i \sim \langle k_\perp^2 \rho_i^2 \rangle$ the finite larmour radius (FLR) parameter (ρ_i is the ion gyroradius and $k_\perp$ the radial wave number); $\langle \ \rangle$ represents a velocity average.

We first note that ion bounce averaging is invalid. As a first approximation we assume that all ions are confined in cells (no passing ions). We further neglect axial variations inside cells. Thus the profiles are all piecewise constant in z with jumps at cell interfaces.

The electron collision frequency is modelled by a Krook collision operator[7]. A Krook operator is used because the general collision operator is a second order elliptic differential operator , and is not analytically tractable. Using

a simple pitch-angle scattering operator alone is not reasonable in a regime where drag and pitch-angle scattering compete. At large collision frequencies, the system is near maxwellian and so are its perturbations. When this is the case, a Krook operator is a reasonable choice for a collision operator that embraces both the effects of drag and pitch-angle scattering. The mirror system we describe is modelled as three coupled cells. Since the Krook operator is algebraic, the resulting dispersion equation is just the determinant of a matrix, whose zeros are easily found numerically, and, in limiting cases, analytically. Had we used a differential operator, we would have had a set of coupled differential equations, which would have been very hard to treat.

Since the collision frequency is high, we assume that the zero-order distribution of the electrons and the ions is maxwellian (the ion collisionality is ignored in the problem, but it is about 10^4 $\sec^{-1}$ which is large enough to force the zero order distribution to relax to a maxwellian). We also assume that the hot electron distribution is maxwellian (the roots are not sensitive to the nature of the hot electron distribution, and this is a convenient assumption).

The zero order axial and radial density and potential profiles are also time dependant. However, their shapes evolve slowly compared to the mode we are studying and are assumed frozen in this analysis.

We study the (azimuthal) $m = 1$ mode, because it is not FLR stabilized, and because it is the primary mode observed in the experiment. We assume the mode to be rigid[8] and alter the drift kinetic equations accordingly.

Clearly the model has many approximations, which limit the useful parameter range. For example, the ion collision frequency is $\nu_i \sim 10^4 \, \mathrm{sec}^{-1}$. Since the ion collisionality is neglected, if a growth rate $\gamma \leq 10^4 \, \mathrm{sec}^{-1}$ is computed, this value is probably in error. Similarly, ignoring the communication of ions between cells, ignoring non-maxwellian deviations in the zero-order distributions, etc, limit the applicability of the results.

III The Dispersion Equation

We begin with the drift kinetic equation[9] for any of N species

$$f = -\frac{q\phi n_0}{T} g_0 + J_0 h \tag{1}$$

$$-i(\omega - \overline{\omega_d})h = -J_0\overline{\nu(h - g_0\tilde{n})} - i(\omega - \omega_*)\frac{qn_0g_0}{T}J_0\overline{\phi} \tag{2}$$

where f is is the first order distribution function, h is the nonadiabatic part of f, q is the charge of the species, T is its (uniform) temperature, n_0 is its density, g_0 is the density normalized maxwellian for the species, J_0 is the zero order Bessel function of the first kind, ϕ is the first order perturbed potential, $\tilde{n} \equiv \int h d^3v$ is the integrated nonadiabatic density, $\overline{(\ )}$ refers to bounce averaging over the appropriate orbit and ω_d, ω_* and ν were defined earlier. The Krook collision operator used is $C(f) = -\nu(h - g\tilde{n})$, which is particle conserving but not momentum or energy conserving.

The J_0 terms appear due to averaging the motion along the exact orbit as opposed to averaging at the guiding centre. But for a rigid mode, these FLR terms vanish except for the polarization drift terms. Keeping only the polarization drift, we obtain the equations

$$f = -\frac{q\phi n_0}{T} g_0(1 + b) + h \tag{3}$$

$$-i(\omega - \overline{\omega_d})h = -\overline{\nu(h - g_0\tilde{n})} - i(\omega - \omega_*)\frac{qn_0g_0}{T}\overline{\phi} \tag{4}$$

where $b = 1 - J_0^2 \sim k_\perp^2\rho_i^2$. We close the system by using quasineutrality

$$\sum_j q_j \delta n_j = 0 \tag{5}$$

where $\delta n \equiv \int f d^3v$ and the subscript $j$indexes species. For clarity we use the following convention regarding indices

$j, j', j''...$ *are species subscripts*
$k, k', k''...$ *are cell subscripts*
$l, l', l''...$ *are velocity space region subscripts*

Then (3), (4) and (5) become

$$f_{jkl} = -\frac{q_j \phi_k n_{0jk}}{T_j} g_{0j}(1 + b_{jkl}) + h_{jl} \tag{6}$$

$$\begin{aligned} -i(\omega - \overline{\omega_{d_j l}})h_{jl} = &- \sum_{k'(l)} \nu_{jk'l}(h_{jl} - g_{0j}\tilde{n}_{jk'})\tau_{jk'l} \\ &- i(\omega - \omega_{*j})\frac{q_j n_{0jk} g_{0j}}{T_j} \sum_{k'(l)} \phi \tau_{jk'l} \end{aligned} \tag{7}$$

$$\sum_j q_j \delta n_{jk} = 0 \tag{8}$$

where τ_{jkl} is the fraction of time spent in velocity region l of cell k by species j. In terms of τ_{jkl}, bounce averaging is written as $\overline{\alpha_{jl}} = \sum_{k'(l)} \alpha_{jk'l}\tau_{jk'l}$ where $\alpha_{jk'l}$ is any bounce averageable quantity, and $\sum_{k'(l)}$ is a sum over cells reached by particles of velocity space region l.

We solve for h_{jkl} in (7)

$$\begin{aligned} h_{jkl} = &\frac{1}{-i(\omega - \overline{\omega_{d_j l}}) + \overline{\nu_{jl}}} \left[g_{0j} \sum_{k'(l)} \nu_{jk'l}\tau_{jk'l}\tilde{n}_{jk'} \right. \\ &\left. - i(\omega - \omega_{*j})\frac{q_j n_{0jk} g_{0j}}{T_j} \sum_{k'(l)} \phi_{k'}\tau_{jk'l} \right] \end{aligned} \tag{9}$$

We then integrate over velocity space and use $\tilde{n} \equiv \int h d^3v$

$$\begin{aligned}\tilde{n}_{jk} &\equiv \sum_l \int_{lk} d^3v h_{jkl} \\ &= \sum_{k'l} \tilde{n}_{jk'} \int_{lk} d^3v \frac{g_{0j}\nu_{jk'l}\tau_{jk'l}}{-i(\omega - \overline{\omega_{djl}}) + \overline{\nu_{jl}}} \\ &\quad + \sum_{k'l} \left(\frac{-iq_j n_{0jk}\phi_{k'}}{T_j} \right) \int_{lk} d^3v \frac{(\omega - \omega_{*j}) g_{0j}\tau_{jk'l}}{-i(\omega - \overline{\omega_{djl}} + \overline{\nu_{jl}})}\end{aligned} \tag{10}$$

where lk under the integral sign represents the region of integration, region l in cell k. The velocity integrals in (10) can be done to give

$$\tilde{n}_{jk} + \sum_{k'} A_{jkk'} \tilde{n}_{jk'} = \sum_{k'} B_{jkk'} \phi_{k'} \tag{11}$$

where

$$A_{jkk'} = -\sum_l \int_{lk} d^3v \frac{i\nu_{jk'l}\tau_{jk'l(k)} g_{0j}}{(\omega - wdbarjl) + i\overline{\nu_{jl}}} \tag{12}$$

$$B_{jkk'} = \frac{q_j n_{0jk}}{T_j} (\omega - \omega_{*j}) \sum_l \int_{lk} d^3v \frac{\tau_{jk'l(k)} g_{0j}}{(\omega - \overline{\omega_{djl}}) + i\overline{\nu_{jl}}} \tag{13}$$

and $\tau_{jk'l}(k)$ is the fraction of time spent in cell k' by a particle belonging to velocity region l in cell k.

If we ignore velocity dependances of quantities and just use their averaged values (12) and (13) become

$$A_{jkk'} = -\sum_l \frac{i\nu_{jk'l}\tau_{jk'l(k)}\eta_{jkl}}{\omega - \overline{\omega_{djl}} + i\overline{\nu_{jl}}} \tag{14}$$

and

$$B_{jkk'} = \frac{q_j n_{0jk}}{T_j} (\omega - \omega_{*j}) \sum_l \frac{\tau_{jk'l(k)}\eta_{jkl}}{\omega - \overline{\omega_{djl}} + i\overline{\nu_{jl}}} \tag{15}$$

where quantities like $\tau_{jk'l(k)}$ now refer to "average" values, and η_{jkl} is the passing or trapped fraction defined by

$$\eta_{jkl} = \int_R d^3v g_{0j}$$

where R is the appropriate region in velocity space. It turns out (Appendix A) that (14) and (15) are good approximations of (12) and (13) for large thermal barriers. We will use these simplified equations when performing perturbation analysis in the next section. Equation (8) can be expanded to get

$$-e^2\phi_k \sum_j \frac{n_{0jk}}{T_j}(1+b_{jk}) + \sum_j q_j \tilde{n}_{jk} = 0 \tag{16}$$

where

$$b_{jk} = \int_R d^3v g_{0j} b$$

For purely magnetically confined systems with uniform mirror ratios, (14) and (15) are correct to first order in $\omega_d/(\omega + i\nu)$. For the case of a collisionless species, equations (11) - (13) simplify to

$$\tilde{n}_{jk} = \sum_k B_{jkk'}\phi_{k'} \tag{17}$$

$$B_{jkk'} = \frac{q_j n_{0jk}}{T_j}(\omega - \omega_{*j}) \sum_l \int_R d^3v \frac{g_{0j}\tau_{jk'l(k)}}{\omega - \overline{\omega_{djl}}} \tag{18}$$

The problem at hand involves collisional electrons and collisionless ions and collisionless hot electrons. So on substituting (17) into (16) for ions and hot electrons we get

$$\begin{aligned} \tilde{n}_{ek} = &-e\phi_k\{\frac{n_{0ek}}{T_e} + \frac{n_{0ik}}{T_i}(1+b_{ik}) + \frac{n_{0hk}}{T_h}\} \\ &+ \sum_{k'} B_{ikk'}\phi_{k'} - \sum_{k'} B_{hkk'}\phi_{k'} \end{aligned} \tag{19}$$

Here we have ignored b_e and b_h as being small. Using (11) we have

$$\sum_{k'} B_{ekk'}\phi_{k'} = \sum_{k'}(\delta_{kk'} + A_{ekk'})\tilde{n}_{ek'}$$

$$= \sum_{k'}(\delta_{kk'} + A_{ekk'})\left[-\phi_{k'}\{\frac{n_{0ek'}}{T_e} + \frac{n_{0hk'}}{T_h} + \frac{n_{0ik'}}{T_i}(1 + b_{ik'})\}\right.$$

$$\left. + \sum_{k''} B_{ik'k''}\phi_{k''} - \sum_{k''} B_{hk'k''}\phi_{k''}\right] \tag{20}$$

where $\delta_{kk'}$ is the kronekker delta function. The ions and hot electrons also completely trapped, so $B_{ikk'}$ and $B_{hkk'}$ are diagonal. This allows us to simplify (20) to

$$\sum_{k'} D_{kk'}\phi_{k'} = \sum_{k'}\left[d_{k'}(\delta_{kk'} + A_{ekk'}) - B_{ekk'}\right]\phi_{k'} = 0 \tag{21}$$

where

$$d_k = -e\frac{n_{0ek}}{T_e} - e\frac{n_{0ik}}{T_i}\{1 + b_{ik} + \int d^3v \frac{\omega - \omega_{*i}}{\omega - \omega_{dik}}\} - e\frac{n_{0hk}}{T_h}\{1 + \int d^3v \frac{\omega - \omega_{*h}}{\omega - \omega_{dhk}}\} \tag{22}$$

For the approximate version corresponding to 14 and 15 this becomes

$$d_k = -e\frac{n_{0ek}}{T_e} - e\frac{n_{0ik}}{T_i}\{b_{ik} + \frac{\omega_{*i} - \omega_{dik}}{\omega - \omega_{dik}}\} - e\frac{n_{0hk}}{T_h}\{\frac{\omega_{*h} - \omega_{dhk}}{\omega - \omega_{dhk}}\} \tag{23}$$

The dispersion equation is then

$$\det D = 0\,. \tag{24}$$

$A_{ekk'}$ and $B_{ekk'}$ are given by (12) and (13) and well approximated by (14) and (15).

IV Perturbation Analysis

We perform a perturbation analysis on (21) of the previous section. For this we order the quantities in the equations and write

$$D_{kk'} = D^{(0)}_{kk'} + \epsilon D^{(1)}_{kk'} + \dots \tag{25}$$

Then we solve the system order by order. To lowest order

$$[\det D_{kk'}]^{(0)} = \det D^{(0)}_{kk'} = 0 \tag{26}$$

yields the roots $\omega^{(0)}_i, i = 1, \dots, n$ (n is the number of roots). We expand $D^{(0)}$ about $\omega^{(0)}_i$ to get correction terms:

$$D^{(0)}_{kk'}(\omega) = D^{(0)}_{kk'}(\omega^{(0)}_i + \epsilon\omega^{(1)}_i + \dots)$$

So

$$\det D^{(0)}_{kk'}(\omega) = \det D^{(0)}_{kk'}(\omega^{(0)}_i) + \epsilon\omega^{(1)}_i \partial_\omega (\det D^{(0)}_{kk'}(\omega))|_{\omega=\omega^{(0)}_i} + \dots$$

We then obtain from the order ϵ equation corresponding to (21)

$$\epsilon\omega^{(1)}_i = -\frac{[\det D_{kk'}(\omega)]^{(1)}}{\partial_\omega(\det D^{(0)}_{kk'}(\omega))}|_{\omega=\omega^0_i} \tag{27}$$

By looking at different regimes of parameters, we get different expansions (25) and so different roots of (26) and their perturbations (27).

1. Limit of zero collisionality

We consider first the limits of zero collisionality ($\nu = 0$) and very small passing fractions ($\eta_e \ll b, \omega_d/\omega_*$), where the usual ordering of the FLR and

drift frequencies ($b, \omega_d/\omega_* \ll 1$) is assumed. (21) becomes ($A_e \equiv 0$ when $\nu = 0$)

$$D_{kk'} = d_{k'}\delta_{kk'} - B_{ekk'} \tag{28}$$

ie.,

$$\begin{aligned} D_{kk'} =& \frac{en_{0ke}}{T_e}\frac{\omega_{*e}-\omega_{dke}}{\omega-\omega_{dke}} + \frac{en_{0ki}}{T_e}\{\hat{b}_k - \frac{\omega_{*e}-\omega_{dke}}{\omega-\omega_{dki}}\} \\ &+ \frac{en_{0kh}}{T_e}\frac{\omega_{*e}-\omega_{dke}}{\omega-\omega_{dkh}} + \eta_{ek}\frac{en_{0ek}}{T_e}\frac{\omega-\omega_{*e}}{\omega-\omega_{dek}} \\ &- \tau_{ek}\eta_{ek}\frac{en_{0ek}}{T_e}\frac{\omega-\omega_{*e}}{\omega-\overline{\omega_{dep}}}, \qquad k = k' \\ D_{kk'} =& -\tau_{ek'}\eta_{ek}\frac{en_{0ek}}{T_e}\frac{\omega-\omega_{*e}}{\omega-\overline{\omega_{dep}}}, \qquad k \neq k' \end{aligned} \tag{29}$$

where $\hat{b} \equiv b_i T_e/T_i$. In cells 1 and 3, $\eta_e \to 0$. In cell 2, η_e can be large or small depending on the barrier. If no hot electrons are present, then $\eta_e \to 0$ in this cell as well.

We first examine a system having no hot electrons. In this case,

$$D^{(0)}_{kk'} = \delta_{kk'}\frac{en_{0ke}}{T_e}\{\frac{\omega_{*e}-\omega_{dke}}{\omega-\omega_{dke}} - \frac{\omega_{*e}-\omega_{dke}}{\omega-\omega_{dki}} + \hat{b}_k\} \tag{30}$$

is diagonal ($\vartheta(D^{(0)}_{kk}) = \vartheta(\omega_d/\omega_*, \hat{b})$). The six roots are MHD-like:

$$\omega^{(0)}_{k\pm} \cong \pm\left[\frac{-\omega_{*e}(\omega_{dek}-\omega_{dik})}{\hat{b}_k}\right]^{\frac{1}{2}} \tag{31}$$

The $\vartheta(\epsilon)$ part of $\det D$ is

$$[\det D]^{(1)} = D^{(0)}_{11}D^{(0)}_{22}D^{(1)}_{33} + D^{(1)}_{11}D^{(0)}_{22}D^{(0)}_{33} + D^{(0)}_{11}D^{(1)}_{22}D^{(0)}_{33} \tag{32}$$

with

$$D^1_{kk} = \eta_{ek}\frac{en_{0ek}}{T_e}\frac{\omega-\omega_{*e}}{\omega-\omega_{dek}} - \eta_{ek}\tau_{ek}\frac{en_{0ek}}{T_e}\frac{\omega-\omega_{*e}}{\omega-\overline{\omega_{dep}}}$$

So (27) gives

$$\omega_{k\pm}^{(1)} \cong -\frac{(1-\tau_{ek})}{2}(\omega_{k\pm}^{(0)} - \omega_{*e})\frac{\eta_{ek}}{\hat{b}_k} \tag{33}$$

Equations (31) and (33) are valid for both two and three cell systems, if we neglect the hot electron effects. When hot electrons are present in cell 2, the zero order roots are as before

$$D_{kk}^{(0)} = 0 \tag{34}$$

However $D_{kk'}^{(0)}$ is no longer diagonal. So the $\vartheta(\epsilon)$ expression in the determinant is changed to

$$\begin{aligned}(\det D)^{(1)} =& D_{11}^{(1)}D_{22}^{(0)}D_{33}^{(0)} - D_{12}^{(1)}D_{21}^{(0)}D_{33}^{(0)} + D_{11}^{(1)}D_{22}^{(0)}D_{33}^{(0)} \\ & - D_{32}^{(1)}D_{11}^{(0)}D_{23}^{(0)} + D_{11}^{(0)}D_{22}^{(0)}D_{33}^{(1)}\end{aligned} \tag{35}$$

We shall not consider the roots in the hot electron cell itself but rather the effect of the hot electrons on the roots in the other cells. We find, for $k = 1, 3$

$$\omega^{(1)} = -\left[\frac{D_{kk}^{(1)}}{D_{kk}^{(0)'}} - \frac{D_{k2}^{(1)}D_{2k}^{(0)}}{D_{22}^{(0)}D_{kk}^{(0)'}}\right] \tag{36}$$

where $(')$ refers to differentiation with respect to ω. Explicitly we find

$$\begin{aligned}\omega^{(1)} =& -\frac{(1-\tau_{ek})}{2}(\omega^{(0)} - \omega_{*e})\frac{\eta_{ek}}{\hat{b}_k} \\ & + \eta_{ek}\tau_{e,4-k}\frac{(\omega^{(0)} - \omega_{*e})^2(\omega^{(0)})^2(\omega - \omega_{dh2})}{4\beta_{h2}\omega_{dek}\omega_{dh2}(\omega_{*e})^2}\end{aligned} \tag{37}$$

The second term represents the modification due to the hot electrons present in cell 2. This result is valid only for large thermal barriers (small passing fractions), so that nearly all the electrons in the middle cell are hot electrons.

The results (33) and (37) allow us to predict for the passing fraction needed for stabilization. The mode stabilizes when its growth rate vanishes, that is when

$$\mathrm{Im}(\omega^{(1)}) = -\mathrm{Im}(\omega^{(0)}) \tag{38}$$

The left hand side is a function of η_1 (or alternatively, of ϕ_2). So we solve for η_1, which yields a condition for the stabilization of the trapped particle mode,

$$\eta_{1,cr} \cong \frac{2\hat{b}_1}{1-\tau_{e1}} \tag{39}$$

Both (33) and (37) yield approximately the above result, since the corrections in (37) are small.

The mode structure is obvious from the diagonal nature of $D^{(0)}$. The mode is strongly localized in cell k. Quantitatively,

$$\left|\frac{\phi_1}{\phi_3}\right| \cong \left|\frac{D^{(0)}_{33}}{D^{(1)}_{31}}\right| \gg 1$$

2. Collisional cells

For this case we have the ordering $(\eta, b, \omega_d/\omega_* \ll 1)$, with the collisionality parameter ν/ω_* arbitrary, and with $\eta, b, \omega_d/\omega_*$ allowed to be of comparable magnitude. The dispersion matrix is

$$D_{kk} = \left[\beta_{ek} + \hat{b}_k - \frac{\omega_{*e} - \omega_{dke}}{\omega - \omega_{dki}} + \beta_{hk}\frac{\omega_{*e} - \omega_{dke}}{\omega - \omega_{dkh}}\right]\left[\frac{\omega - \omega_{dek} + i\nu_{ek}\eta_k}{\omega - \omega_{dek} + i\nu_{ek}} - \frac{i\nu_{ek}\tau_{ek}\eta_k}{\omega - \overline{\omega_{dep}} + i\overline{\nu_e}}\right]$$

$$- \beta_{ek}(\omega - \omega_{*e})\left[\frac{1-\eta_k}{\omega - \omega_{dek} + i\nu_{ek}} + \frac{\eta_k\tau_{ek}}{\omega - \overline{\omega_{dep}} + i\overline{\nu_e}}\right] \tag{40}$$

$$D_{kk'} = -\left[\beta_{ek'} + \hat{b}_{k'} - \frac{\omega_{*e} - \omega_{dk'e}}{\omega - \omega_{dk'i}} + \beta_{hk'}\frac{\omega_{*e} - \omega_{dk'e}}{\omega - \omega_{dk'h}}\right] \times \frac{i\nu_{ek'}\tau_{ek'}\eta_k}{\omega - \overline{\omega_{dpe}} + i\overline{\nu_e}} - \beta_{ek}(\omega - \omega_{*e})\frac{\eta_k\tau_{ek'}}{\omega - \overline{\omega_{dpe}} + i\overline{\nu_e}}$$

Here β_{ek} and β_{hk} are the fraction of cold and hot electrons in cell k respectively. Equation 40 can be rewritten as follows

$$D_{k,k'} = (d_k + e_k\eta_k)\delta_{k,k'} + \eta_k\tau_{k'}f_{k'} \tag{41}$$

where

$$d_k = \left(\frac{\omega - \omega_{dek}}{\omega - \omega_{dek} + i\nu_{ek}}\right)\left[\hat{b}_k + \frac{\beta_{ek}\omega_{*e}(\omega_{dek} - \omega_{dik})}{(\omega - \omega_{dek})(\omega - \omega_{dik})} + \frac{\beta_{hk}[\omega_{*e}(\omega_{dhk} - \omega_{dik}) + \omega_{dhk}\omega_{dek}]}{(\omega - \omega_{dek})(\omega - \omega_{dhk})}\right] \tag{42}$$

$$e_k = \left[\beta_{ek} + \hat{b}_k - \frac{\omega_{*e} - \omega_{dek}}{\omega - \omega_{dik}} + \beta_{hk}\frac{\omega_{*e} - \omega_{dek}}{\omega - \omega_{dhk}}\right]\frac{i\nu_{ek}\eta_k\delta_{k,k'}}{\omega - \omega_{dek} + i\nu_{ek}} + \beta_{ek}(\omega - \omega_{*e})\frac{\eta_k\delta_{k,k'}}{\omega - \omega_{dek} + i\nu_{ek}} \tag{43}$$

$$f_k = -\left[(\beta_{ek} + \hat{b}_k - \frac{\omega_{*e} - \omega_{dek}}{\omega - \omega_{dik}} + \beta_{hk}\frac{\omega_{*e} - \omega_{dek}}{\omega - \omega_{dhk}})\frac{i\nu_{ek}}{\omega - \overline{\omega_{d+}i\nu_e}} + \beta_{ek}\frac{(\omega - \omega_{*e})}{\omega - \overline{\omega_{d+}i\nu_e}}\right] \tag{44}$$

The determinant of the dispersion equation 41 can then be written down

$$(\det D) = (d_1 + e_1\eta_1)(d_2 + e_2\eta_2)(d_3 + e_3\eta_3)\left[1 + \sum_{k=1}^{3}\frac{\eta_k\tau_k f_k}{d_k + e_k\eta_k}\right] = 0 \tag{45}$$

To observe qualitative features, we simplify by choosing $\nu_{ek} \equiv \nu$, $\hat{b}_k \equiv \hat{b}$ in all cells. For a two cell analogue, the hot electron cell is replaced by a velocity space barrier, which simply changes the number of passing electrons. Then to first order in $\eta, b, \omega_d/\omega_{*e}$, for a system of two cells, the equations become

$$\det D = c_1c_2 + (\omega - \omega_{*e})(\omega + i\nu)(c_1\frac{\tau_1}{\eta_1} + c_2\frac{\tau_2}{\eta_2})\eta_1\eta_2 \tag{46}$$

where

$$c_k = \hat{b}\omega^2 + \omega_{*e}(\omega_{dek} - \omega_{dik}) \tag{47}$$

For a three cell analogue, with the middle cell at a lower potential with respect to the end cells, but with no hot electrons present,

$$\begin{aligned}\det D =& c_1c_2c_3 \\ &+ (\omega - \omega_{*e})(\omega + i\nu)\left[c_1c_2(1 - \tau_3)\eta_3\right. \\ &\qquad \left. + c_2c_3(1 - \tau_1)\eta_1 + c_3c_1(1 - \tau_2)\eta_2\right] \\ &+ (\omega - \omega_{*e})^2(\omega + i\nu)^2\left[c_1\frac{\tau_1}{\eta_1} + c_2\frac{\tau_2}{\eta_2} + c_3\frac{\tau_3}{\eta_3}\right]\eta_1\eta_2\eta_3\end{aligned} \tag{48}$$

Both (46) and (48) show how the roots depend on the passing fraction. When $\eta \ll \hat{b}, \omega_d/\omega_{*e}$ we recover the case of weakly coupled cells (ie, we get both (30) and (31) from the above expressions), which we have already examined. If we allow $\eta \gg \hat{b}, \omega_d/\omega_{*e}$ then we find double roots at ω_{*e} and $-i\nu_e$ and a pair of MHD-like roots for a pressure weighted, curvature driven mode. To see the last, we note that these roots correspond to

$$\sum_{i=1}^{cells} c_i \frac{\tau_i}{\eta_i} \cong 0 \tag{49}$$

In (49), τ_i measures (approximately) the length of the cell and $1/\eta$ represents the ratio of the overall density to the passing fraction density. So (49) represents a density weighted equation. Since T is assumed uniform, this is equivalent to saying that (49) represents a pressure weighting of the drive. So if the system is net MHD stable, then these roots should also be stable.

Equations (46) and (48) are quartic and hexic respectively and so cannot be solved exactly (actually (46) can be solved, but the solution is not illuminating). But we can solve them approximately. This enables us to look at the behaviour of the roots in the region $\eta \gg \hat{b}, \omega_d/\omega_{*e}$. We examine the two unperturbed solutions

$$\omega_1^0 = \omega_{*e} \qquad\qquad \omega_2^0 = \overline{\omega} \tag{50}$$

where $\overline{\omega}$ is the positive real solution of (49). Perturbing these roots then yields (only the results for the three cell systems are given)

$$\omega_1^1 = \left(\frac{-\omega_{*e} + i\nu_e}{\omega_{*e}^2 + \nu_e^2}\right) \left[\frac{c_1(\omega_{*e})c_2(\omega_{*e})c_3(\omega_{*e})}{\eta_1\eta_2\eta_3} \frac{\sum_{j'} \frac{\eta_{j'}(1-\tau_{j'})}{c_{j'}(\omega_{*e})}}{\sum_j \frac{c_j(\omega_{*e})\tau_j}{\eta_j}}\right] \tag{51}$$

and

$$\omega_2^1 = \left(\frac{-\overline{\omega} + i\nu_e}{\overline{\omega}^2 + \nu_e^2}\right)\left[\frac{c_1(\overline{\omega})c_2(\overline{\omega})c_3(\overline{\omega})}{2\hat{b}\overline{\omega}(\overline{\omega} - \omega_{*e})}\frac{\sum_i \frac{(1-\tau_i)\eta_i}{c_i(\overline{\omega})}}{\tau_1\eta_2\eta_3 + \tau_2\eta_3\eta_1 + \tau_3\eta_1\eta_2}\right] \qquad (52)$$

where the c_i were defined in (47). The coefficients in (51) and (52) are such that in the MMX parameter range, both roots are growing (or unstable) solutions. In general, the sign of the quantities in the square brackets in (51) and (52) determines the nature of the roots.

The critical (stabilizing) value of η_1 in the limit $\nu \to 0$, can be calculated from (51) and (52). We find that the roots $\omega^{(0)} = 0$ and $\omega^{(0)} = +\overline{\omega}$ collide and move into the complex plane. The value of η_{cr} at which this is occurs can be got from

$$\left|\frac{\sum_{1,2,3} c_1(0)c_2(0)(1-\tau_3)\eta_3}{\omega_{*e}\sum_{1,2,3} c_1(0)\tau_1\eta_2\eta_3}\right| + \left|\frac{\sum_{1,2,3} c_1(\overline{\omega})c_2(\overline{\omega})(1-\tau_3)\eta_3}{(\overline{\omega} - \omega_{*e})\overline{\omega}^2\sum_{1,2,3}\hat{b}\tau_1\eta_2\eta_3}\right| = \overline{\omega} \qquad (53)$$

where the $\sum_{1,2,3}$ represents cyclic summations over $1, 2, 3$.

To examine the effect of hot electrons, we can look directly at equations (41) to (45). The case of weakly coupled cells has already been treated at the beginning of the section. We now go to the other limit. Suppose the cells are very strongly coupled. Then the thermal barrier is weak, and there are very few hot electrons. We expand (45) to first order in β_h, $\hat{b}$ and ω_d/ω. The equations are very complicated, and so we assume that ν_e and $\hat{b}$ are independant of position. Then we get

$$\sum_{k=1}^{3}\frac{\tau_k}{\eta_k}(\omega^2+\gamma_k^2)-\frac{\beta_h\tau_2}{\hat{b}}\left[-(\omega+i\nu)(\omega-\omega_{*e})\frac{i\nu\omega\omega_{*e}}{\omega-\omega_{dh}}\right.$$
$$\left.-\frac{\omega\omega_{*e}\omega_{dh}}{\omega-\omega_{dh}}\frac{1}{\eta_2}+\omega(\omega-\omega_{*e})+i\nu\omega\frac{\omega-\omega_{*e}-\omega_{dh}}{\omega-\omega_{dh}}\right]\cong 0 \tag{54}$$

When the coupling dominates, the roots tend towards $\overline{\omega}$. The presence of the weak barrier causes a shift in the eigen frequency which is easily calculated from the above equation. We find for the residual growth rate

$$\gamma=\frac{1}{\sum_{k=1}^{3}\frac{\tau_k}{\eta_k}}\frac{\beta_h\tau_2}{\hat{b}}\frac{\nu\omega_{*e}}{\overline{\omega}};. \tag{55}$$

This is valid only when the collision frequency is not much larger than $\overline{\omega}$ for that could promote first order variables into zero order. The growth rate got here must be added to the growth rate obtained from ignoring hot electrons (52), since those terms have been ignored here.

V Results and Comparison with Experiment

1. Numerical Computation

Equation (21) in section III was solved numerically and the various roots obtained. For each group of particles present, there is a root to track. In the three-cell configuration there are eight such groups (three groups each of trapped, cold electrons and ions, a group of trapped hot electrons and a group of passing electrons). This yields eight roots to track, of which six are stable. One of the remaining roots is the curvature-driven trapped particle mode and the other is a drift mode. Although both of these modes are unstable, the trapped particle mode is the dominant (ie., most unstable) mode for small and medium passing fractions, and both modes are only weakly unstable at large passing fractions.

In fig. 2 we show a typical root locus of the trapped particle mode as the passing fraction is varied. At small values of the passing fraction the mode structure is well localised to the unstable cell. As the passing fraction increases, there is a stabilizing influence from the other cells. The mode becomes global and tends towards a mode frequency and a mode structure that corresponds to the system-averaged MHD mode.

In fig. 3 we show a family of root loci versus the passing fraction, that is parametrized by the collision frequency ν. We see that the reduction in growth rate with increasing passing fraction is initially more rapid at higher collisionalities. At large passing fractions, the collisional processes dominate and the growth rate scales with $\nu/(\overline{\omega}^2 + \nu^2)$.

In fig. 4, we compare the results of the numerical solutions with perturbation theory for the case of two cells with a barrier separating them. As seen in the figure there is little qualitative difference. The only change that is significant is the increased time spent by transiting electrons in stable regions for the three cell case. This produces stabilization at a lower electron passing fraction.

2. Comparison of Numerical Results with the Experiment

In this section we compare the predictions of the theory with the available evidence for the MMX experiment. The experimental set-up and the experimental parameters were described in sec II. A more complete description of the experiment and initial experimental results are given in ref [6]. Here we present some additional experimenatl results and compare these results with the theory. In both the original experimental results and the results presented here, the following observations can be made In fig. 5, the radial component of the velocity of the centroid motion is plotted for successive times separated by ten microseconds and averaged over three points taken two microseconds apart. Values are only plotted for radially outward motion. The velocity is converted to an effective growth rate using the relationship

$$\gamma = \frac{1}{r_w}\frac{\mathrm{d}r}{\mathrm{d}t} \tag{56}$$

where r_w is the plasma radius matched to an assumed Gaussian. This form is justified in ref [6]. In fig. 5a the result is shown for the basic configuration of two stable and one unstable cell without applying the ECRH pulse. The motion shown is in the magnetically unstable cell. The effective γ is found to lie below $10^5\ \mathrm{sec}^{-1}$. In fig. 5b the result is given for a fully stabilized magnetic field with ECRH applied to the middle cell at time zero. Again the effective γ lies essentially below $10^5\ \mathrm{sec}^{-1}$. In fig. 5c the basic configuration with one unstable cell is again used with the ECRH applied at t = 0. There is a definite increase in the effective growth rate after heating, and the plasma is found to move rapidly to the chamber wall. It appears to bounce off the

wall without extreme loss of density, and after 50μsec, which is the time for the barrier to decay settles down again to a value below $10^5\,\mathrm{sec}^{-1}$.

From data such as that shown in fig. 5 and that given in [6] we can make the following qualitative statements:

(1) When no barrier is present, and the system is calculated to be MHD stable when taken as a whole, there is no observed instability on the order of the experiment time($\approx 10\mu$sec).

(2) When a barrier is suddenly formed, the magnetically unstable cell is observed to become unstable, with the plasma quickly lost radially. The time scale for the plasma loss is $\leq 10\mu$sec.

(3) The theory predicts small growth rates at large passing fractions (no barrier present) and also predicts that the bad curvature cell becomes flute unstable at small passing fraction (large barrier present). The actural growth rate depends on γ_{MHD} in this cell, which depends on the drive and the temperatures of the various populations present. Using the experimental estimates of $T_e \sim 15\mathrm{eV}$, $T_i \sim 5\mathrm{eV}$, $\omega_d \sim 3 \times 10^3\,\mathrm{sec}^{-1}$ (unstable) gives us $\gamma_{MHD} \sim 1.2 \times 10^5\,\mathrm{sec}^{-1}$. This value is somewhat lower than the observed loss time. The values of ω_d and T_e above are rather uncertain and it is quite possible that this value of γ_{MHD} is as high as $5 \times 10^5\,\mathrm{sec}^{-1}$, which would be reasonably consistent with the observations.

(4) The plasma restabilizes after about 50μsec, coinciding with the decay of the potential barrier.

(5) If the unstable cells are stabilized with quadrupole fields, the residual motion remains after ECRH but no significant increase in velocity is found and the plasma does not move radially outwards to the device walls.

In fig. 6 we plot the numerical values of γ for the parameters most closely matching the experiment, but allowing the passing fraction to vary. On this plot we superpose the estimated experimental effective growth rates as scaled from the observed velocity of the plasma centroid. We superpose experimental values right after heating when we expect the barrier to be essentially $4T_e$, after some barrier decay, and after nearly complete decay of the barrier. We see that even in this last case in the passing fraction is considerably less than unity, and the mode growth is substantial. Nevertheless, the actual plasma motion appears to be saturated, with the centroid confined near the magnetic axis. The complete motion is shown is some detail in our previous paper. We conclude that the theory is consistent qualitatively with the experimentally observed decoupling of the stable and unstable cells in the presence of an ECRH induced potential barrier.

VI Conclusions

A simple formalism has been derived in this paper to handle mirror systems that consist of many coupled regions. It assumes that the bounce frequency of ions is smaller than the mode frequency and approximates them as being completely confined to the region they are in. The potential barriers separating regions are assumed to be driven by hot electrons. The cold electrons are assumed to have a bounce frequency large compared to the mode frequency.

The resulting equations are found to agree with the experimental observations of the trapped particle mode on the MMX.

The most serious approximation in the model is the assumption that the ions are completely confined and that the mode is uniform within a cell. A more sophisticated approach is being developed that takes the ion dynamics into account, allows the mode to vary within a cell, and can use any bounce averaged electron response. This should be of relavence to the current generation of mirror systems, which have relatively cold ions, with transit times longer than the mode period.

A Large Thermal Barriers

We evaluate (12) and (13), in the limit of small $\omega_d/(\omega-\omega_*)$. The integrals take the form

$$I_l = \sum_{k'(l)} \alpha_{k'} \int_{R_{kl}} d^3v \frac{\tau_{jk'l} g_{0jk}}{\omega + i\overline{\nu_{jl}}} \left(1 + \sum_{k''(l)} \frac{\omega_{djk''}\tau_{jk''l}}{\omega + i\overline{\nu_{jl}}}\right) \tag{57}$$

where $\omega_{djk''} = \frac{m}{2}\omega_{djk''0}(v_\parallel^2 + \frac{1}{2}v_\perp^2)$ with $\omega_{djk''0}$ constants. We also take the Krook collision frequency to be the same in all cells. Then we need to evaluate integrals of the type

$$J_{lkk'} = \int_{R_{kl}} d^3v \tau_{jk'l} g_{0jk} \tag{58}$$

$$K_{lk'k''} = \int_{R_{kl}} d^3v \tau_{jk'l}\tau_{jk''l} g_{0jk}\omega_{djk''l} \tag{59}$$

Evaluation is best done in the $(u-\mu)$ coordinates, where

$$\mu = \frac{1}{2}\frac{mv_\perp^2}{B} \qquad\qquad u = \frac{E - \mu B_0 - \Phi_2}{\Phi_2} \tag{60}$$

where Φ_2 is the potential energy gain of an electron when it enters cell 2 from cell 1. In these coordinates,

$$\begin{aligned} g_{01}d^3v &= \frac{\sqrt{\pi\Phi_2}}{B_0\beta^{3/2}}\left(\frac{du}{\sqrt{u+1}} \wedge d\mu\right) \\ g_{02}d^3v &= \frac{e^{-\beta\Phi_2}\sqrt{\pi\Phi_2}}{B_0\beta^{3/2}}\left(\frac{du}{\sqrt{u}} \wedge d\mu\right) \end{aligned} \tag{61}$$

where $\beta = 1/T$. For the trapped region, the integration is straightforward, and we get (for $\Phi_2 \gg T$)

$$I_{jk} = \alpha_{jk}\eta_{jk}\frac{1}{\omega + i\overline{\nu} - \omega_{djk0}T)} + \vartheta(e^{-\beta\Phi_2}\frac{\omega_d\alpha_{jk}}{\omega + i\nu}) \tag{62}$$

Hence when we have a large barrier we can perform this integral by just replacing the variable quantities by their averages.

For passing particles, we need to evaluate integrals of the type (58) and (59). In $u-\mu$ coordinates

$$\tau_1 = \tau_3 = \frac{\sqrt{u}}{2\sqrt{u}+\sqrt{u+1}} \qquad \tau_2 = \frac{\sqrt{u+1}}{2\sqrt{u}+\sqrt{u+1}} \tag{63}$$

To evaluate (58) and (59), we approximate (63) by

$$\begin{aligned} \tau_1 = \tau_3 &= \begin{cases} .645\sqrt{u} - .346u & 0 \le u < 1 \\ \dfrac{1}{3} - \dfrac{1}{24u} & u \ge 1 \end{cases} \\ \tau_2 &= \begin{cases} 1 - 1.29\sqrt{u} + .692u & 0 \le u < 1 \\ \dfrac{1}{3} + \dfrac{1}{12u} & u \ge 1 \end{cases} \end{aligned} \tag{64}$$

This approximation has a maximum error of .025. Using the following formulae

$$\int_0^1 d^3v v^k e^{-\alpha v^2} = \begin{cases} \dfrac{n!}{2\alpha^{n+1}}\left[1 - e^{-\alpha}\sum_{j=0}^{n}\dfrac{\alpha^j}{j!}\right] & ,k = 2n+1 \\ \dfrac{(2n-1)!!}{(2\alpha)^n}\left[\dfrac{1}{2}\sqrt{\dfrac{\pi}{\alpha}}\right. & \\ \qquad \left. -\dfrac{e^{-\alpha}}{2\alpha}\sum_{j=0}^{n}\dfrac{(2j)^j}{(2j-1)!!}\right] & ,k = 2n, \alpha \to \infty \end{cases} \tag{65}$$

$$\int_1^\infty du \frac{e^{-\alpha u}}{\sqrt{u}} = \frac{e^{-\alpha}}{\alpha} \qquad \alpha \to \infty \tag{66}$$

$$\int_1^\infty du \frac{e^{-\alpha u}}{u\sqrt{u}} = \vartheta\frac{e^{-\alpha}}{\alpha^2} \qquad \alpha \to \infty \tag{67}$$

$$\int_1^\infty du \frac{e^{-\alpha u}}{u^2\sqrt{u}} = \frac{2}{3}e^{-\alpha} \qquad \alpha \to \infty \tag{68}$$

we find that

$$\langle \tau_k \rangle \equiv \frac{\int_P d^3v \tau_k g_{0k}}{\int_P d^3v g_{0k}} = \begin{cases} .73\sqrt{\dfrac{T}{\Phi_2}} - .52\dfrac{T}{\Phi_2} + \cdots & k = 1,3 \\ 1 - 1.46\sqrt{\dfrac{T}{\Phi_2}} + 1.04\dfrac{T}{\Phi_2} + \cdots & k = 2 \end{cases} \tag{69}$$

When we evaluate (59) and use (69), we find that

$$\langle \omega_{dk''} \tau_{k'} \tau_{k''} \rangle \cong \Omega_{k''} \langle \tau_{k'} \rangle \langle \tau_{k''} \rangle \tag{70}$$

where

$$\Omega_k = \begin{cases} \omega_{dk0}\Phi_2 & k = 1,3 \\ 2\omega_{dk0}T & k = 2 \end{cases} \qquad (\Phi_2 \gg T) \tag{71}$$

Clearly then, for $\Phi_2 \gg T$, (57) becomes

$$\begin{aligned} I_l &\cong \sum_{k'(l)} \alpha_{k'} \int_{R_{kl}} d^3v \frac{\langle \tau_{jk'l} \rangle g_{0jk}}{\omega + i\nu - \langle \overline{\omega_d} \rangle} + \cdots \\ &\cong \sum_{k'(l)} \alpha_{k'} \eta_{pk} \frac{\langle \tau_{k'} \rangle}{\omega + i\nu - \overline{\omega}\rangle} \end{aligned} \tag{72}$$

which gives us (14) and (15).

Acknowledgement

The authors would like to thank R.H. Cohen for his help in formulating the model, and J.C.Fernandez and C.P.Chang for their help in defining the experimental setup in such a way that modelling was possible. The work was partially supported by the United States Department of Energy under DOE Contract DE-FG0386ER51103.

References

[1] H.L.Berk, M.N.Rosenbluth, H.V.Wong, T.M.Antonsen and D.E.Baldwin, Fiz. Plasmy 9, 176 (1983) (English Version).

[2] R.H.Cohen, W.M.Nevins and H.L.Berk, Phys. Fluids 29(5), 1578 (1986).

[3] H.L.Berk, M.N.Rosenbluth, R.H.Cohen and W.M.Nevins, Phys. Fluids 28(9), 2824 (1985).

[4] H.L.Berk, M.N.Rosenbluth, H.V.Wong, T.M.Antonsen, D.E.Baldwin, B.Lane, Plasma Phys. and Controlled Nucl. Fus. Research 1982, p175, Vol II (IAEA) Vienna,1983.

[5] B.Lane, Phys. Fluids 29(5), 1532 (1985).

[6] J.C.Fernandez, C.P.Chang, A.J.Lichtenberg, M.A.Lieberman and H.Meuth, Phys. Fluids 29(4), 1208 (1986).

[7] P.L.Bhatnagar, E.P.Gross and M.Krook, Phys. Rev. 94, p 511 (1954).

[8] T.B.Kaiser, L.D.Pearlstein, Phys. Fluids 28(3), 1003 (1985); M.N.Rosenbluth, N.A.Krall and N.Rostoker, Nucl. Fusion 1962 suppliment Part 1, 143.

[9] T.M.Antonsen and B.Lane, Phys. Fluids 23(6),1205 (1980).

List of Figures

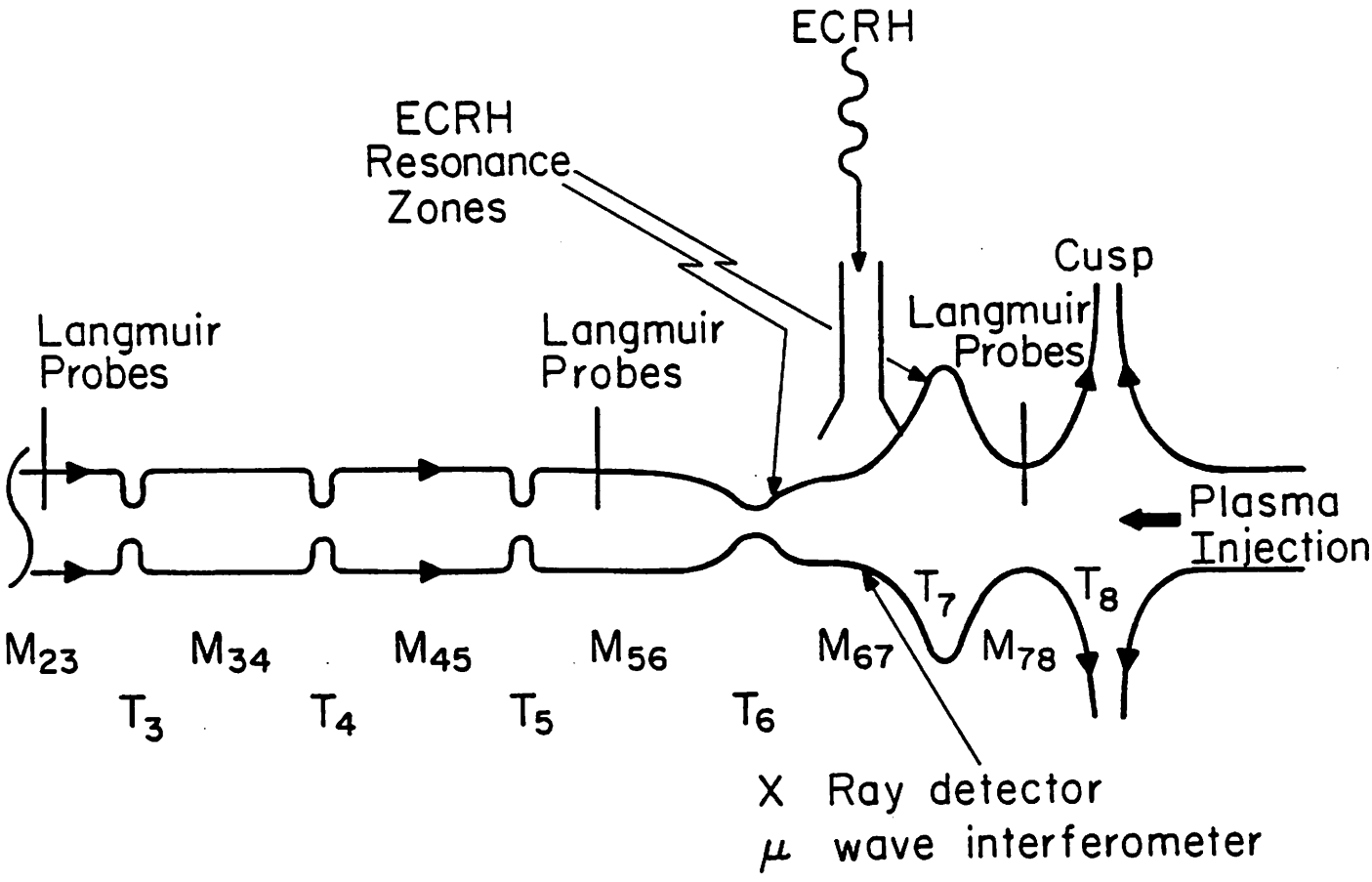
ECRH
ECRH
Resonance
Zones
Cusp
Langmuir
Probes
Langmuir
Probes
Langmuir
Probes
Plasma
Injection
T_7
T_8
M_{23}
M_{34}
M_{45}
M_{56}
M_{67}
M_{78}
T_3
T_4
T_5
T_6
X Ray detector
μ wave interferometer

Fig. 1

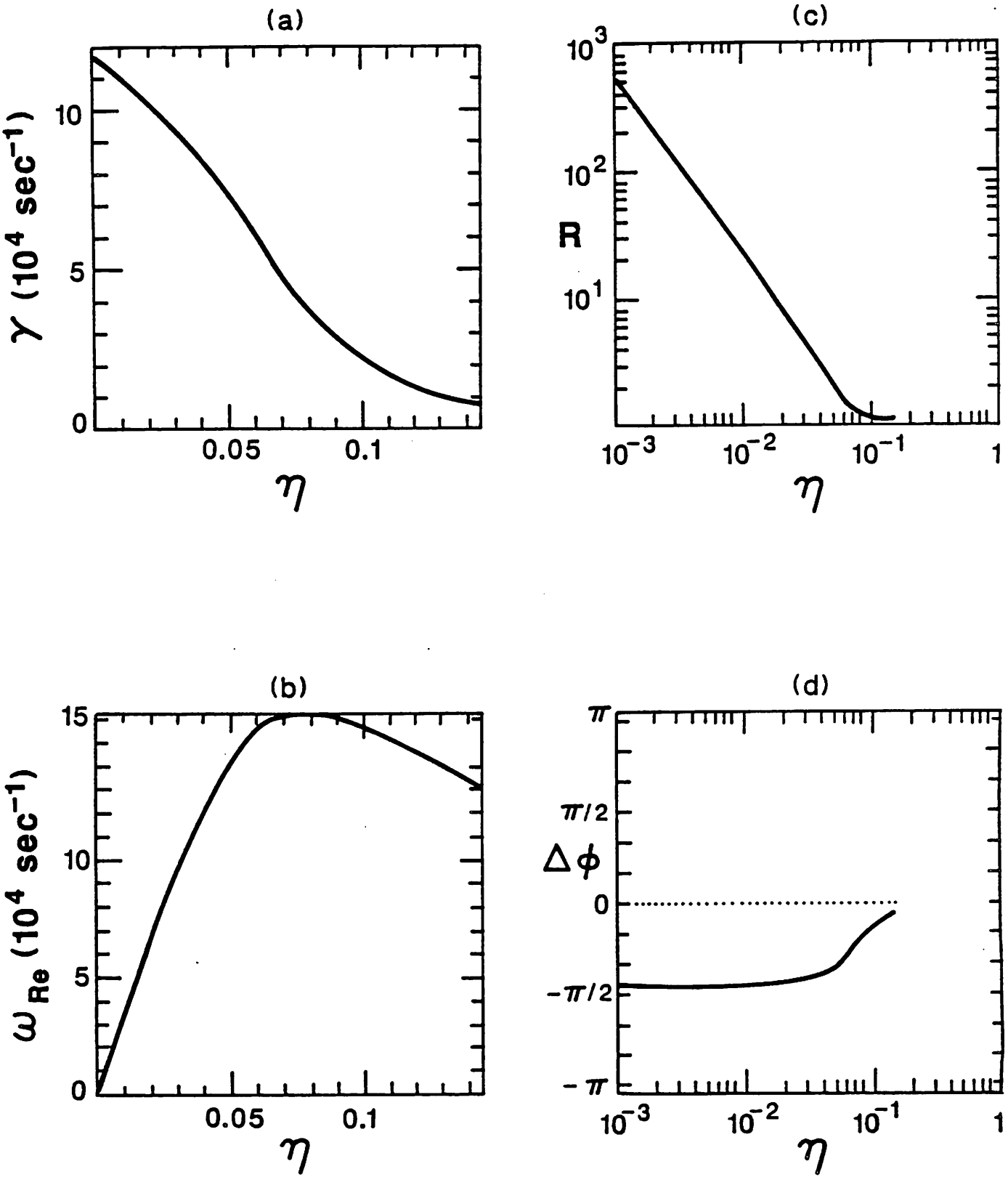
(a)
γ (10^4 sec^{-1})
10
5
0
0.05
0.1
η
(c)
10^3
10^2
R
10^1
10^{-3}
10^{-2}
10^{-1}
1
η
(b)
ω_{Re} (10^4 sec^{-1})
15
10
5
0
0.05
0.1
η
(d)
π
$\pi/2$
$\Delta\phi$
0
$-\pi/2$
$-\pi$
10^{-3}
10^{-2}
10^{-1}
1
η

Fig. 2

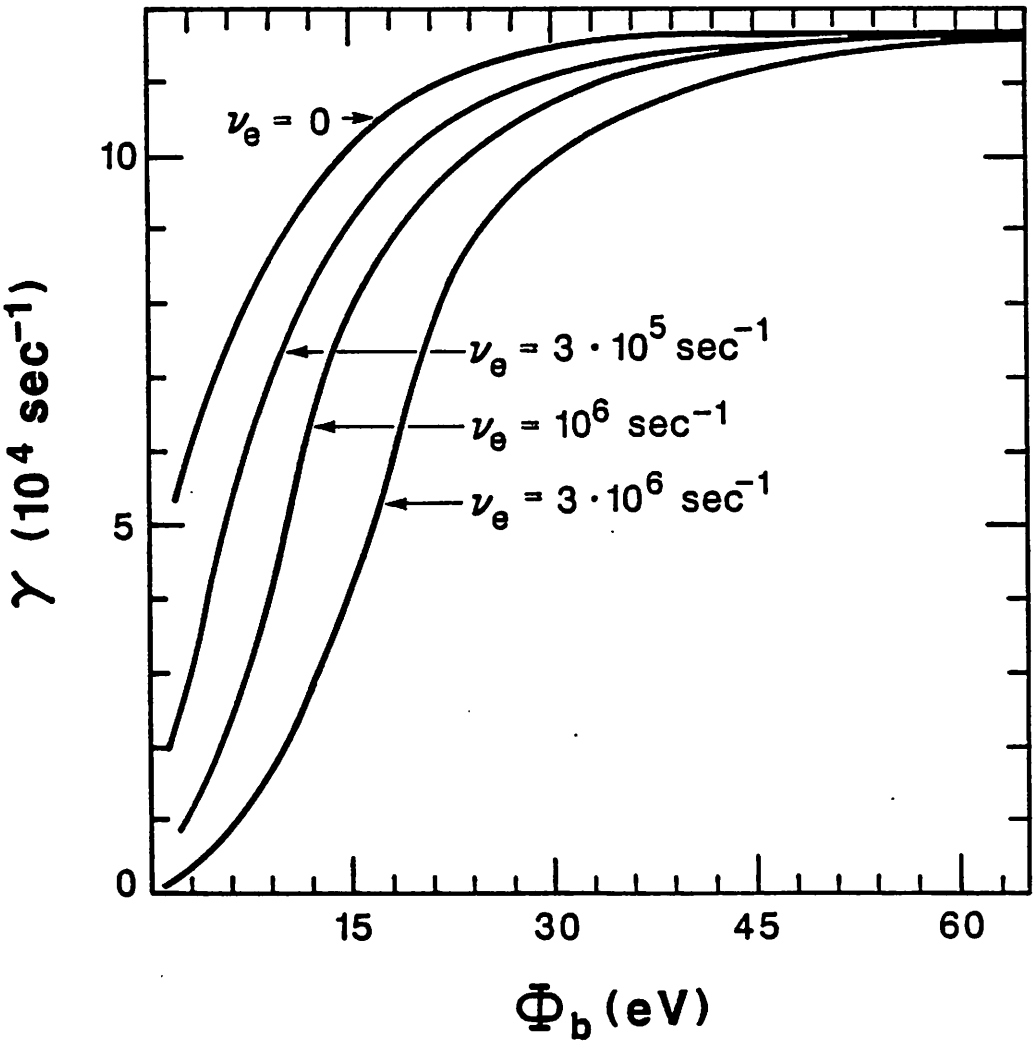
$\nu_e = 0$
$\nu_e = 3 \cdot 10^5\ sec^{-1}$
$\nu_e = 10^6\ sec^{-1}$
$\nu_e = 3 \cdot 10^6\ sec^{-1}$
$\gamma\ (10^4\ sec^{-1})$
10
5
0
15
30
45
60
$\Phi_b\ (eV)$

Fig. 3

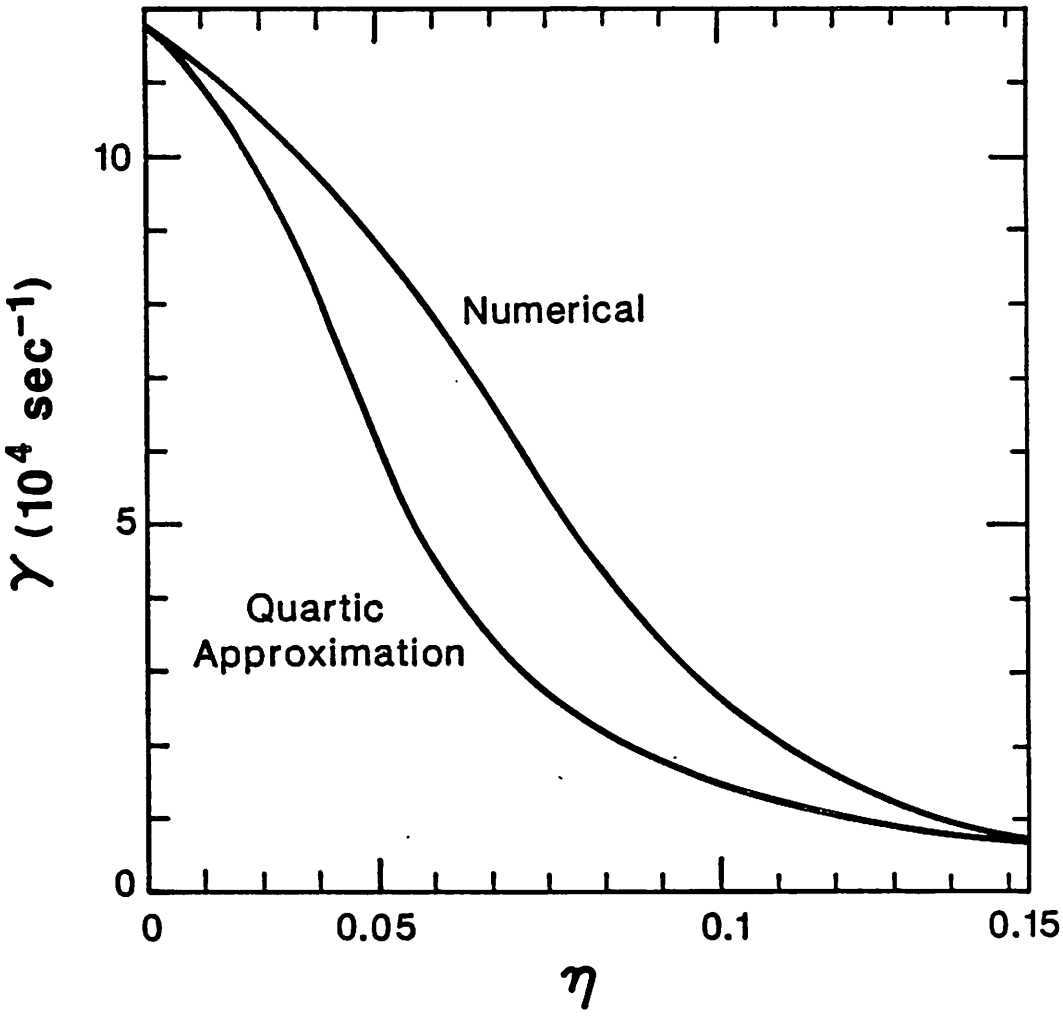
10
5
0
0
0.05
0.1
0.15
γ (10^4 sec^{-1})
η
Numerical
Quartic
Approximation

Fig. 4

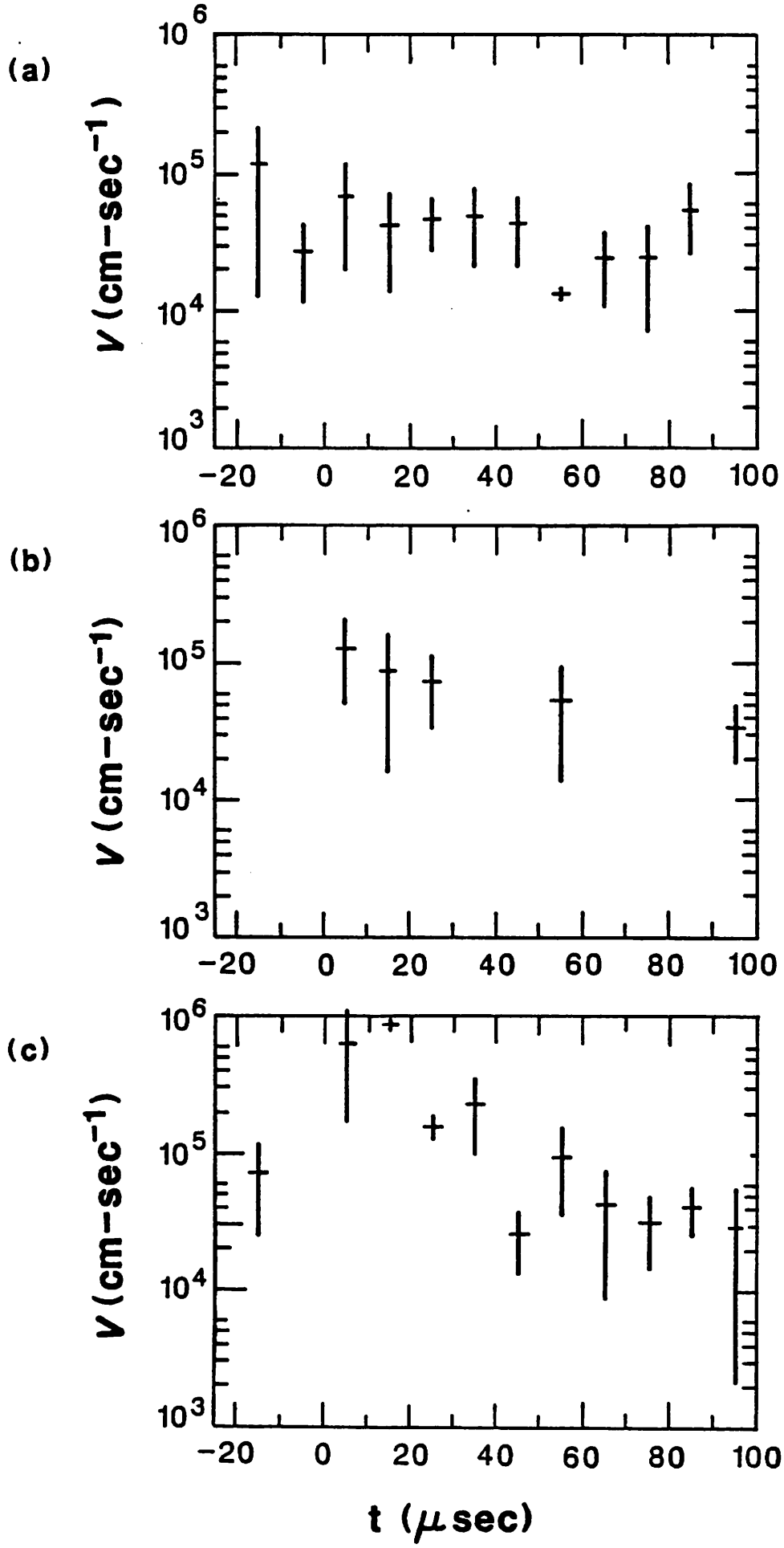

Fig. 5

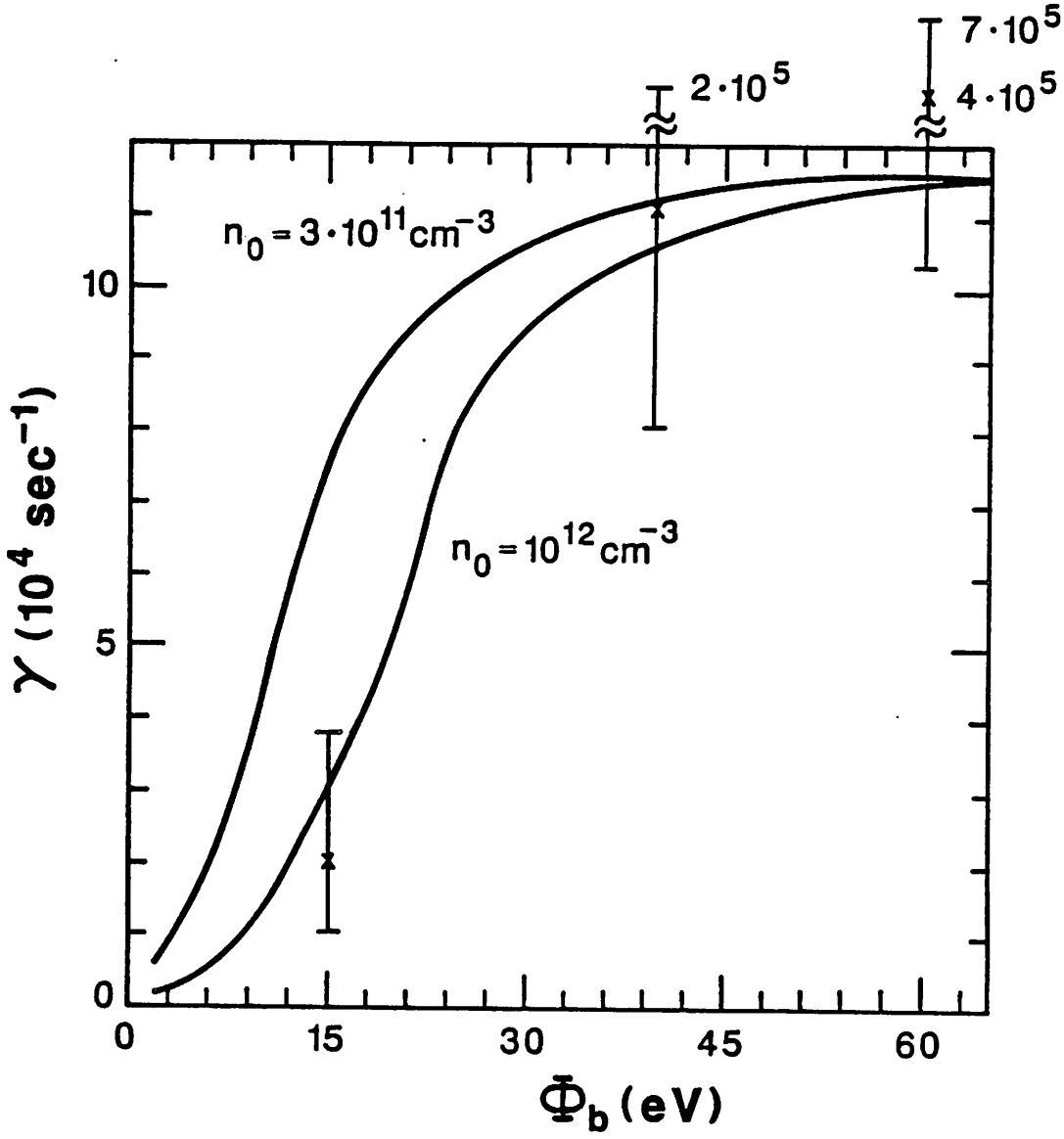
7·10^5
2·10^5
4·10^5
n0 = 3·10^11 cm^-3
n0 = 10^12 cm^-3
γ (10^4 sec^-1)
10
5
0
0
15
30
45
60
Φb (eV)

Fig. 6